

Proceedings of Meetings on Acoustics

Volume 19, 2013

<http://acousticalsociety.org/>



**ICA 2013 Montreal
Montreal, Canada
2 - 7 June 2013**

Signal Processing in Acoustics

Session 1pSPa: Nearfield Acoustical Holography (NAH) Measurements and Applications

1pSPa4. Modified statistically optimized near-field acoustical holography for jet noise characterization

Alan T. Wall*, Kent L. Gee and Traciannne B. Neilsen

***Corresponding author's address: Department of Physics and Astronomy, Brigham Young University, N283 ESC, Provo, Utah 84663, alantwall@gmail.com**

Near-field acoustical holography has been shown to be a useful tool for visualizing jet noise fields. It has been applied to a full-scale jet on an installed military aircraft with promising results, but the source characteristics in the extreme near field have been difficult to characterize because of the interference of acoustic reflections off the rigid reflecting plane beneath the jet. To provide accurate sound field reconstructions, a modified approach to statistically optimized near-field acoustical holography (SONAH) is implemented. In conventional SONAH, the sound field is represented by a matrix of elementary wave functions at all desired spatial locations. In this modified approach, advantage is taken of the property that arbitrary, user-defined functions can be selected for this matrix. Here, two sets of cylindrical wave functions, one centered on the jet centerline and one on the image source centerline, are used to obtain an accurate near-field reconstruction.

Published by the Acoustical Society of America through the American Institute of Physics

1. INTRODUCTION

Preliminary results of applying near-field acoustical holography (NAH) as a method to characterize the noise sources of jets have shown promise. NAH is an inverse technique, wherein sound pressures over a measured surface (the hologram) are represented with an equivalent source model (ESM) or an equivalent wave model (EWM), and the resulting model is used to predict sound pressures elsewhere in the three-dimensional region near the hologram. For example, in one study of a laboratory-scale jet in a free-field environment, the jet was considered a nearly cylindrical radiator, and cylindrical NAH based on an EWM was successfully applied in a straightforward fashion.¹ In another study, an ESM-based NAH algorithm was applied to laboratory-scale jet noise using a conical array of point monopoles, and methods similar to Helmholtz equation least-squares (HELS) holography were applied to reconstruct the far field.² Extension of NAH approaches to full-scale high-performance engine exhaust has only been recently carried out.^{3,4}

There are difficulties in applying NAH to the full-scale jet problem that are not present in laboratory experiments. First, it is difficult to capture the entire field because of the extended nature of the source. Second, the interference effects from the rigid ground plane must be accounted for in the algorithms. In previous work on data collected near an F-22A,^{3,4} two approaches were taken to account for the reflections. First, based on the method of images, the total source region was expanded to include an image source below the ground plane.⁵ The measured data were “mirrored” over the reflecting plane and then projected with planar NAH toward a combined source and image plane near the shear layer.³ The general trends in the sound field were captured using this approach, but the levels in the near field were underestimated. In the second approach, a cylindrical NAH projection was made from a ground-based array, which did not contain spatially dependent interference patterns⁶ (see also Long *et al.*⁷). This provided a more plausible near-field reconstruction than did the planar holography, but an axisymmetric assumption was required.

In the current investigation, the properties of the full-scale jet experiment⁸ are simulated using a numerical line source to create a sound field on a large planar aperture near a rigid reflecting surface. A multisource-type EWM, based on statistically optimized near-field acoustical holography (SONAH), is used to represent the sound field. SONAH is a patch NAH method that was developed for cases where the measurement aperture is limited by physical constraints.⁹ It avoids the direct calculation of the spatial Fourier transform and instead utilizes a transfer function matrix between the measurement and reconstruction locations. Thus, SONAH allows flexibility in the selection of these locations. In addition, it allows for a more convenient representation of the sound field than other NAH algorithms, because multiple sets of wave functions can be included in the generation of the transfer function matrix. Thus, a multisource-type EWM (i.e. the inclusion of multiple wave-function sets) is used in conjunction with the SONAH algorithm to reconstruct the sound field of the numerical source near a reflecting surface.

2. THEORY

Key portions of the SONAH formulation that pertain to this work are provided here. For a comprehensive review of SONAH theory, the reader is directed to the work of Hald⁹ and of Cho *et al.*¹⁰ First, assume a complex time harmonic sound field in a homogeneous medium, measured at a set of positions $\mathbf{r}_h, h = 1, \dots, I$ (the hologram), in a source-free region, Ω . Consider the problem of reconstructing the sound field in Ω from the measured pressures. The field may be approximated by the summation of a set of elementary wave functions (Green’s functions) that fulfill the homogeneous wave equation in Ω , written as

$$p(\mathbf{r}_h) = \sum_{n=1}^N a_n \Phi_n(\mathbf{r}_h), \quad h = 1, \dots, I. \quad (1)$$

Here, there are N wave functions, Φ_n , measured at I hologram locations, and it is desirable to find the complex expansion coefficients, a_n that allow Eq. (1) to accurately represent the field. In an EWM formulation, the wave functions are typically a set of planar, cylindrical, or spherical waves, with a common origin such that conformal surfaces in the coordinate system are nearly parallel to the surface of the radiator. Such a set of wave functions ensures a convenient representation of the true radiation and result in a sufficiently accurate reconstruction, provided other requirements, typical of NAH, are met.

However, for more complicated cases where the sound field is generated by sources of multiple shapes and/or at multiple locations, with an unknown degree of coherence, it may be difficult to find a convenient set of wave functions of a single origin that represent the field. With a rudimentary estimate of source locations and shapes, a set of wave function values at all measurement positions can be defined for the m th source and formulated as the matrix

$$\mathbf{B}_m = \begin{bmatrix} \Phi_1^m(\mathbf{r}_1) & \Phi_1^m(\mathbf{r}_2) & \dots & \Phi_1^m(\mathbf{r}_l) \\ \Phi_2^m(\mathbf{r}_1) & \Phi_2^m(\mathbf{r}_2) & \dots & \Phi_2^m(\mathbf{r}_l) \\ \vdots & \vdots & \ddots & \vdots \\ \Phi_N^m(\mathbf{r}_1) & \Phi_N^m(\mathbf{r}_2) & \dots & \Phi_N^m(\mathbf{r}_l) \end{bmatrix} = [\Phi_n^m(\mathbf{r}_h)]. \quad (2)$$

A similar matrix of wave function values is defined at a desired reconstruction location, \mathbf{r}_r , as $\boldsymbol{\beta}_m = [\Phi_n^m(\mathbf{r}_r)]$. The wave function matrix for all M sources are then concatenated vertically to obtain composite matrices:

$$\mathbf{A} = \begin{bmatrix} \mathbf{B}_1 \\ \mathbf{B}_2 \\ \vdots \\ \mathbf{B}_M \end{bmatrix}, \text{ and } \boldsymbol{\alpha} = \begin{bmatrix} \boldsymbol{\beta}_1 \\ \boldsymbol{\beta}_2 \\ \vdots \\ \boldsymbol{\beta}_M \end{bmatrix}. \quad (3)$$

These complete wave function matrices are then processed, using a traditional SONAH algorithm. In summary, the reconstructed sound pressure at \mathbf{r}_r is given by

$$\mathbf{p}(\mathbf{r}_r) = \mathbf{p}(\mathbf{r}_h)^T \mathbf{R}_{\mathbf{A}^H \mathbf{A}} \mathbf{A}^H \boldsymbol{\alpha}, \quad (4)$$

where $\mathbf{R}_{\mathbf{A}^H \mathbf{A}}$ is the regularized inverse of $\mathbf{A}^H \mathbf{A}$ [see Cho *et al.*¹⁰ Eq. (32)]. The use of multiple sets of elementary wave functions allows fields with complex radiation to be represented conveniently, and provides an accurate reconstruction.

3. EXPERIMENT

In this numerical experiment, the simulated measurement and environment were designed to mimic that of NAH measurements made in the geometric near field of a full-scale jet, including the presence of a rigid reflecting surface.⁸ No attempt was made to provide an equivalent source model of a jet. As illustrated in Figure 1, the source was a linear array of point monopoles that extended from $z = 0$ to $z = 15$ m, at $x = 0$, and a height of $y = 1.9$ m. An identical image source was simulated below the rigid ground-reflection plane (the x - z plane) at $y = -1.9$ m. For each frequency investigated, sources were placed one tenth of a wavelength apart to ensure a dense spacing. A Gaussian weighting was applied to the source array amplitudes, and a phase delay was applied to each source to give the array a directivity of 55° relative to the z -axis. Field values were simulated by applying the monopole Green's function to each source individually and summing. A numerical hologram was simulated over a planar surface at heights between $y = 0.4$ and 2.2 m, and on the diagonal between $(z, x) = (1.6, 6.4)$ and $(24.5, 9.8)$ m. The hologram locations, \mathbf{r}_h were spaced equally in both directions with a spacing of 0.15 m. For each frequency, prior to SONAH propagation, the hologram grid resolution was reduced by removing rows and columns, such that at least two measurements per acoustic wavelength were ensured.

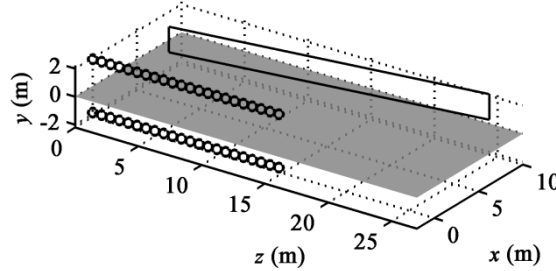


FIGURE 1. Simulation setup. The location of the source array and its image are marked by the circles. The rectangle outlines the hologram location. The gray rectangle represents the rigid reflecting surface.

The modified SONAH algorithm, explained in Section 2, was applied to reconstruct the sound field near the source. In this case, two sets of cylindrical wave functions were used (see Figure 2). Elementary cylindrical wave functions at a given location \mathbf{r} are defined by

$$\Phi_{k_z,n}(\mathbf{r}) = \Phi_{k_z,n}(r, \phi, z) \equiv \frac{H_n^{(1)}(k_r r)}{H_n^{(1)}(k_r r_0)} e^{in\phi} e^{ik_z z}, \quad r \geq r_0, \quad (5)$$

where $H_n^{(1)}$ is the n th-order Hankel function of the first kind, r_0 is some small reference radius (traditionally the assumed source radius), and the radial wavenumber is

$$k_r = \begin{cases} \sqrt{k^2 - k_z^2}, & \text{for } |\mathbf{k}| \geq |k_z|, \\ i\sqrt{k_z^2 - k^2}, & \text{for } |\mathbf{k}| < |k_z|, \end{cases} \quad (6)$$

with $k = \omega/c$ being the angular frequency, and $c = 343$ m/s the ambient sound speed. In this experiment, Hankel functions of order $n = -1$ through 1 were used. Equation (5) was evaluated at all hologram locations with respect to two cylindrical “origins” to form $\mathbf{B}_1 = [\Phi_n^1(|\mathbf{r}_h - \mathbf{r}_0^1|)]$ and $\mathbf{B}_2 = [\Phi_n^2(|\mathbf{r}_h - \mathbf{r}_0^2|)]$, where \mathbf{r}_0^1 defines the line that is collinear with the upper source array, and where \mathbf{r}_0^2 defines the line that is collinear with the lower source array. These were then concatenated to form the complete hologram wave function matrix, \mathbf{A} , as in Equation (3). A similar process was implemented to form the complete reconstruction wave function matrix, $\boldsymbol{\alpha}$. An illustration of the (real) values of two wave functions, each evaluated on a cylindrical surface in one of the respective coordinate systems, is provided in Figure 2. Finally, SONAH was implemented using Equation (4) to reconstruct the near-field pressures. Reconstructions were made over a two-dimensional surface at a uniform height of $y = 1.9$ m (the same height as the top source array), which extended from $x = 0.1$ to 10 m and from $z = 0$ to 30 m.

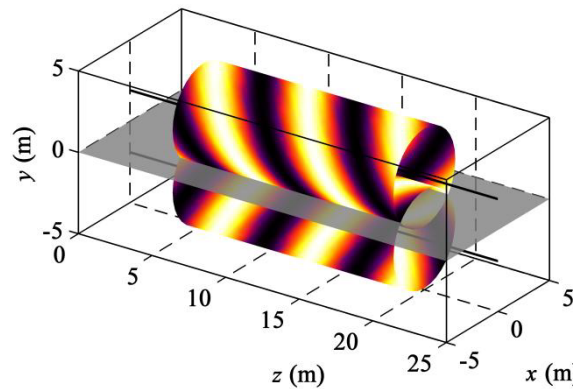


FIGURE 2. Two cylindrical wave functions, which were used in the current simulation, evaluated over cylindrical surfaces in their respective coordinate systems.

To evaluate the accuracy of the modified SONAH algorithm for the current experiment, benchmark values were calculated at the reconstruction locations. In addition, a traditional planar SONAH⁹ and a traditional cylindrical SONAH algorithm,¹⁰ with a single origin collinear with the top source array, were applied to the same data. As a final analysis of the accuracy of the modified SONAH algorithm, reconstructions were performed for several frequencies to determine the frequency range over which this algorithm is successful for the current experiment.

The numerical source arrays here (as well as full-scale jets) represent sources of large extent. For some frequencies, the width of the hologram aperture (in the z direction) was insufficient to prevent large errors that result from edge effects. Hence, several aperture-extension techniques⁵ were applied to the measured data, prior to holographic projection. A linear prediction algorithm¹¹ was used to numerically extend the effective aperture size by about 20 m in both the directions of increasing and decreasing z prior to MSTR SONAH. For the planar SONAH case, the aperture extension process described by Wall *et al.*³ was applied to the data, which includes a “mirror” of the data over the reflecting plane, then outward extrapolation using the analytic continuation method.¹² Prior to the cylindrical SONAH implementation, analytic continuation was applied to extrapolate the data 0.3 m in the positive and negative y directions, and about 20 m in the positive and negative z directions.

4. RESULTS AND DISCUSSION

The sound field from the numerical line array was calculated at a frequency of 125 Hz, which is the octave-band center frequency closest to the peak frequency in a typical full-scale jet spectrum⁸. SONAH reconstructions of the calculated near field are given in Figures 4 and 5. All levels shown are calculated relative to the peak pressure value measured on the hologram, p_{\max} . In addition, the levels that are more than 40 dB below the maximum level (of the benchmark) are excluded from the plot. For each plot, the x -axis is on the right side, with values increasing toward the left. A benchmark from the numerical model is provided in Figure 3a, against which reconstructions of the field can be compared. Note the directionality of the radiation and the presence of a null along $x \approx 4$ m, due to destructive interference from the image source array. The white dashed line marks the location of the vertical hologram, projected onto the x - z plane, for this and subsequent figures. Figure 3b shows the reconstructed field after the implementation of the modified SONAH algorithm, and Figure 3c is a map of the level difference (error) between the benchmark and reconstructed levels. The modified SONAH is able to capture the directivity, interference null, and near-source levels. For all high-amplitude regions (within 20 dB of the maximum) the error is less than 2 dB. For comparison, the alternate SONAH reconstructions are given in Figure 4. Figure 4a shows the near-field reconstruction from planar SONAH, and Figure 4b shows its respective error. Note that, near the source (at $x \approx 0.1$ m), the reconstruction levels underestimate the true levels by more than 10 dB. These demonstrate how planar SONAH does not predict the geometrical spreading (increasing level toward the source) of the field, since the hologram was not close enough to sufficiently capture evanescent wave information in the acoustic near field (see similar results for the physical experiment in Reference 3). In contrast, both the modified SONAH and the cylindrical SONAH reconstructions represent the geometrical spreading. However, the cylindrical SONAH method does not account for interference from the secondary source, and therefore does not capture the interference null and distorts the shape of the source region (see Figure 4c and d).

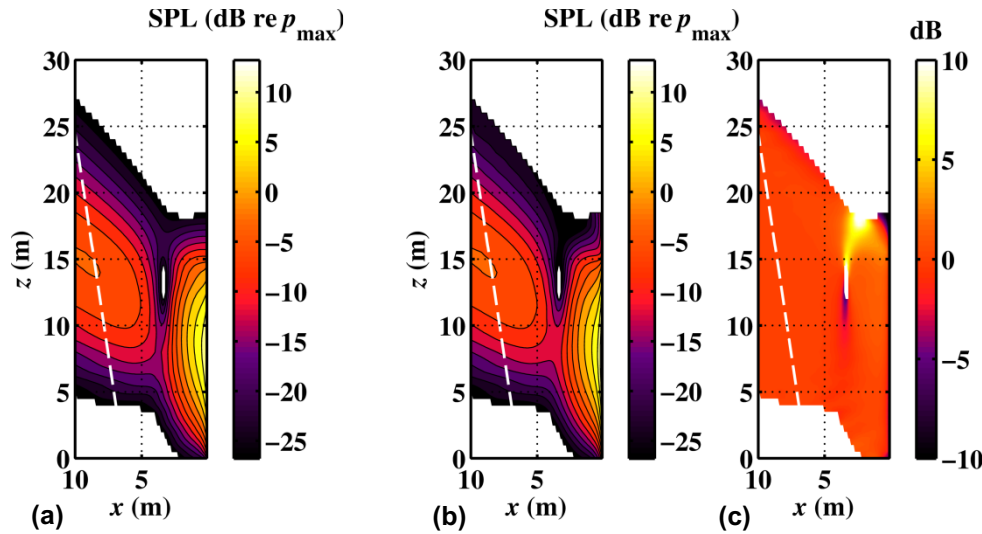


FIGURE 3. Modified SONAH reconstruction of the numerically generated field at a height of $y = 1.9$ m, and at 125 Hz. The projected location of the hologram is marked by the white dashed lines. (a) Benchmark. (b) Reconstruction. (c) Error (dB difference) between the reconstruction and benchmark.

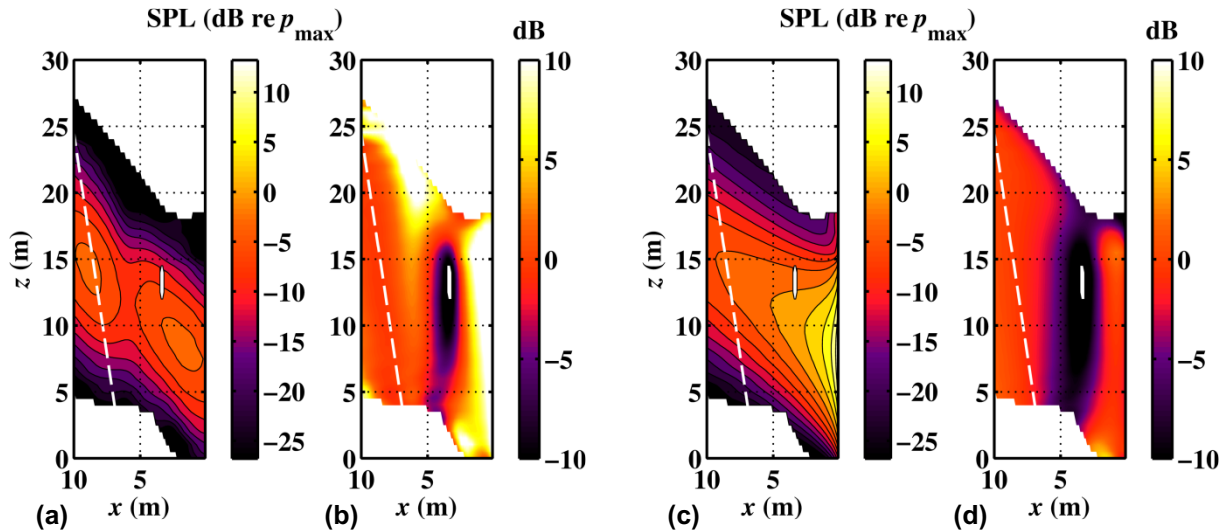


FIGURE 4. Alternate SONAH reconstructions of the numerically generated field at a height of $y = 1.9$ m, and at 125 Hz. The projected location of the hologram is marked by the white dashed lines. (a) Planar SONAH reconstruction. (b) Error (dB difference) between the planar SONAH reconstruction and benchmark. (c) Cylindrical SONAH reconstruction. (d) Error (dB difference) between the cylindrical SONAH reconstruction and benchmark.

To provide a further comparison of the three methods, SONAH reconstructions were repeated for 500 Hz, which is the octave-band center frequency two octaves above 125 Hz. Reconstructed source levels at $y = 1.9$ m and one quarter of an acoustic wavelength from the source are shown in Figure 5. The modified SONAH reconstruction provides a result within 1 dB at all source locations for the 500 Hz case, shown in Figure 5a. In contrast, planar SONAH levels differ by about 10 dB, and cylindrical SONAH levels by about 3 dB at all locations.

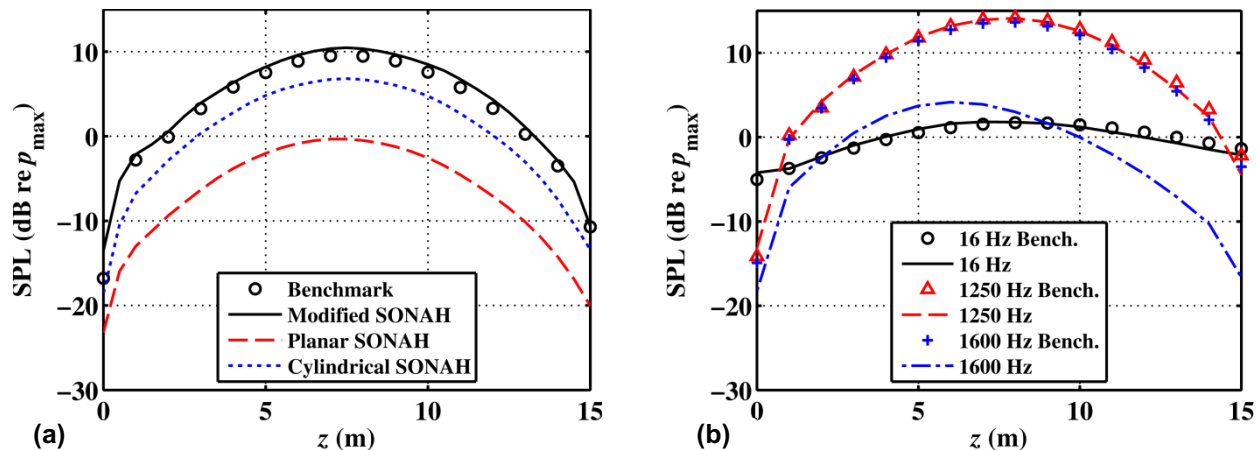


FIGURE 5. (a) Modified, planar, and cylindrical SONAH reconstructions of the numerically generated field at a height of $y = 1.9$ m and one quarter of an acoustic wavelength from the source for 500 Hz. Benchmark values are shown with circles. (b) Modified SONAH reconstructions of the numerically generated field at a height of $y = 1.9$ m and one quarter of an acoustic wavelength from the sources, for 16, 1250, and 1600 Hz. Benchmark levels are shown as symbols.

For future application of acoustical holography to the full-scale jet noise experiment, it is desirable to understand the frequency range over which the modified SONAH method returns a reliable reconstruction. This has been explored for the current numerical line source and hologram geometry. Source reconstructions and their respective calculated benchmarks are shown in Figure 5b for three frequencies. Note that the error for 16 Hz is less than 1 dB, demonstrating that this method can be successfully employed down into the infrasonic range. Figure 5b also shows less than 1 dB error for the reconstruction at 1250 Hz, which is the highest one-third octave band center frequency for which good agreement holds. A reconstruction for the next one-third octave band, 1600 Hz, is also shown, and the error exceeds 10 dB in some locations. This is because the requirement for two sensors per acoustic wavelength on the hologram array is no longer met. In fact, the cutoff frequency for a grid with 0.15 m spacing is 1143 Hz, but because sound waves arrive at less than grazing incidence at the hologram array locations, reconstruction at 1250 Hz is still accurate.

5. CONCLUSION

A modified SONAH method, which allows for a representation of a sound field with a multiple-source equivalent wave model (EWM), was presented in this paper. This method allows for holographic reconstruction of sound fields from multiple sources with various shapes and complicated distributions. It has been applied here in a numerical study that mimics the source and measurement configuration of a full-scale jet experiment, where the jet was located near a rigid reflecting surface.⁸ For many of the frequencies of interest, hologram measurements were not taken sufficiently close to the numerical source to be considered in the acoustic near field; they did not capture significant evanescent wave information for a successful source reconstruction. However, the modified SONAH method was able to reconstruct the directivity, levels, and interference patterns of the near field. For comparison, modified SONAH, traditional planar SONAH and cylindrical SONAH methods have all been employed to reconstruct the same region near the simulated sources. Neither planar nor cylindrical SONAH were able to represent both the geometric spreading and interference patterns of the field. However, modified SONAH, with its ability to mathematically account for the image source, was able to reproduce both of these effects. An investigation of the reliable frequency range has determined that the modified SONAH method can accurately reconstruct the field over seven octaves for this numerical experiment, ranging from the infrasonic regime up to the 1250 Hz one-third-octave band. This cutoff frequency is due to the fact that the hologram must contain two sensors per trace acoustic wavelength.

The multisource-type SONAH method discussed is presented here for the first time. Further investigation is required to quantify how much the aperture extension, described herein, influences the reconstruction accuracy. In addition, the effects of varying the parameters in the SONAH algorithm, such as the Hankel function orders and the range of axial wavenumbers included in the EWM, must be explored. In future work, the modified SONAH method will be applied to the full-scale jet experiment data.

ACKNOWLEDGMENTS

The authors would like to thank Michael Muhlestein for his insightful contributions. Alan T. Wall was funded in part by an appointment to the Student Research Participation Program at U.S. Air Force Research Laboratory, Human Effectiveness Directorate, Warfighter Interface Division, Battlespace Acoustics administered by the Oak Ridge Institute for Science and Education through an interagency agreement between the U.S. Department of Energy and USAFRL.

REFERENCES

- ¹M. Lee and J. S. Bolton, "Source characterization of a subsonic jet by using near-field acoustical holography," *J. Acoust. Soc. Am.* **121**, 967-977 (2007).
- ²P. N. Shah, H. Vold and M. Yang, "Reconstruction of far-field noise using multireference acoustical holography measurements of high-speed jets," *AIAA Paper 2011-2772*, June 5-8, 2011.
- ³A. T. Wall, K. L. Gee, T. B. Neilsen, D. W. Krueger, M. M. James, S. D. Sommerfeldt and J. D. Blotter, "Full-scale jet noise characterization using scan-based acoustical holography," *AIAA Paper 2012-2081*, June 4-6, 2012.
- ⁴A. T. Wall, K. L. Gee and T. B. Neilsen, "On near-field acoustical inverse measurements of partially coherent sources," *Proc. Mtgs. Acoust.* **11**, 040007 (2012).
- ⁵A. T. Wall, K. L. Gee, D. W. Krueger, T. B. Neilsen and S. D. Sommerfeldt, "Aperture extension for near-field acoustical holography of jet noise," *Proc. Mtgs. Acoust.* **14**, (pending submission).
- ⁶D. W. Krueger, *Array-based characterization of military jet aircraft noise* (M.S. Thesis, Brigham Young University, Provo, 2012).
- ⁷D. Long, J. Peters and M. Anderson, "Evaluating turbofan exhaust noise and source characteristics from near field measurements," *AIAA Paper 2009-3214*, May 11-13, 2009.
- ⁸A. T. Wall, K. L. Gee, M. M. James, K. A. Bradley, S. A. McInerny and T. B. Neilsen, "Near-field noise measurements of a high-performance military jet aircraft," *Noise Control Eng. J.* **60**, 421-434 (2012).
- ⁹J. Hald, "Basic theory and properties of statistically optimized near-field acoustical holography," *J. Acoust. Soc. Am.* **125**, 2105-2120 (2009).
- ¹⁰Y. T. Cho, J. S. Bolton and J. Hald, "Source visualization by using statistically optimized near-field acoustical holography in cylindrical coordinates," *J. Acoust. Soc. Am.* **118**, 2355 (2005).
- ¹¹R. Scholte, I. Lopez, N. B. Roozen and H. Nijmeijer, "Truncated aperture extrapolation for Fourier-based near-field acoustic holography by means of border-padding," *J. Acoust. Soc. Am.* **125**, 3844-3854 (2009).
- ¹²E. G. Williams, "Continuation of acoustic near-fields," *J. Acoust. Soc. Am.* **113**, 1273-1281 (2003).